GENERATING A BIOACTIVE PROTEIN GRADIENT ON ELECTROSPUN NANOFIBER MATS USING A BOVINE SERUM ALBUMIN BLOCKING SCHEME

A Dissertation
Presented to
The Academic Faculty

by

Michael Luciano Tanes

In Partial Fulfillment
of the Requirements for the Degree
Master of Science in the
School of Biomedical Engineering

Georgia Institute of Technology
Emory University
December 2016

GENERATING A BIOACTIVE PROTEIN GRADIENT ON ELECTROSPUN NANOFIBER MATS USING A BOVINE SERUM ALBUMIN BLOCKING SCHEME

Approved by:

Dr. Younan Xia, Advisor
School of Biomedical Engineering
Georgia Institute of Technology

Dr. Edward Botchwey
School of Biomedical Engineering
Georgia Institute of Technology

Dr. Zhiqun Lin
School of Materials Science and Engineering
Georgia Institute of Technology

Date Approved: November 1, 2016

To my parents, Regina and Alex, for their ongoing love, support, and patience.

ACKNOWLEDGEMENTS

I would like to thank my advisor, Dr. Younan Xia, for allowing me the opportunity to work in his laboratory. I would also like to thank my committee members, Dr. Edward Botchwey and Dr. Zhiqun Lin, for their cooperation in this endeavor. I thank all of the past and present Xia group members for their ideas, assistance with my research, and friendship. Special consideration goes to Dr. Jiajia Xue for her work with the DRG study and helping me greatly with putting together a manuscript. I would also like to give a special thanks to Dr. Kyle Gilroy and Jianhua Li with whom I was able to work closely on some other projects that helped me branch out and learn about nanoparticle synthesis, characterization, and application.

Finally, I have to thank my friends and family. Without their support, I would not have managed to come this far. I do not know how to express the depth of my gratitude for everything you all have done for me, so I hope this might serve as a small token until I figure it out.

TABLE OF CONTENTS

LIST OF TABLES

LIST OF FIGURES

LIST OF SYMBOLS AND ABBREVIATIONS

ABAM	Antibiotic antimycotic
BSA	Bovine serum albumin
c_{max}	Maximum fluorescent intensity
c_0	Initial fluorescent intensity
DCM	Dichloromethane
DMF	Dimethylformamide
DRG	Dorsal root ganglion
ECM	Extracellular matrix
FITC	Fluorescein isothiocyanate
GFP	Green fluorescent protein
HBSS	Hank's buffered salt solution
NGF	Nerve growth factor
PBS	Phosphate buffered saline
PCL	Polycaprolactone
PF	Pyridinium formate
SEM	Scanning electron microscopy
T_m	Time to half maximum coverage

SUMMARY

Electrospun nanofibers are valuable tools in tissue engineering given the possibilities to mimic various ECM architectures. However, the incorporation of biochemical cues remains a significant issue. The biggest challenge is replicating the protein gradients that inspire and direct cell behavior during many of the body's processes. A procedure was developed to generate a bioactive protein gradient on nanofiber mats. The proposed approach was facile, robust, and conserved the amount of bioactive protein needed to produce a gradient. BSA adsorption to PCL nanofibers was found to be a time- and concentration-dependent process. By increasing the volume of solution in a container over time, a BSA gradient was generated across the length of a strip of nanofibers. Vacancies left by the adsorbed BSA on the nanofiber surface were filled-in by a small volume of bioactive protein solution. To test the efficacy of this proposed gradient-generating scheme, DRG isolated from chick embryos were cultured on aligned PCL nanofibers with NGF adsorbed homogeneously or as a gradient. DRG on homogeneously adsorbed NGF scaffolds extended neurites of equal length on either side of the DRG cell mass. However, on the scaffolds with an NGF gradient, the neurites extending towards the increasing NGF concentration were significantly longer than neurites extending against the gradient.

CHAPTER 1. INTRODUCTION

1.1 Background

Protein gradients have profound effects on the body during wound healing, normal growth and development, and disease generation and progression. For example, chemoattractant gradients can encourage and direct the growth of peripheral nerves in the developing fetus, guide immune cells to sites of injury or infection, and attract blood vessels to hypoxic tumors.[1-4] In the area of regenerative medicine, the ability to direct and influence cell migration, differentiation, or extension with protein gradients is a potentially powerful tool to improve tissue regeneration rate.[5-7]

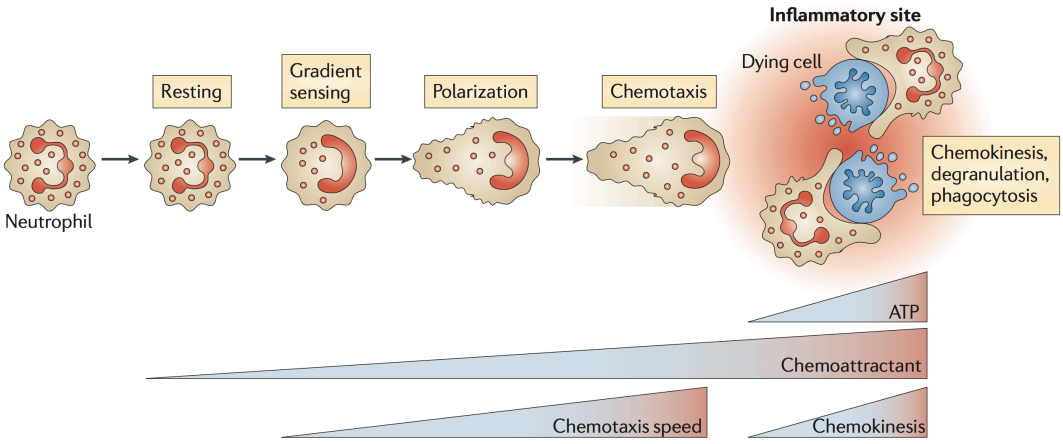

Figure 1. A cell responds to a chemoattractant gradient by first sensing, then polarizing with, and finally migrating along the gradient.[3]

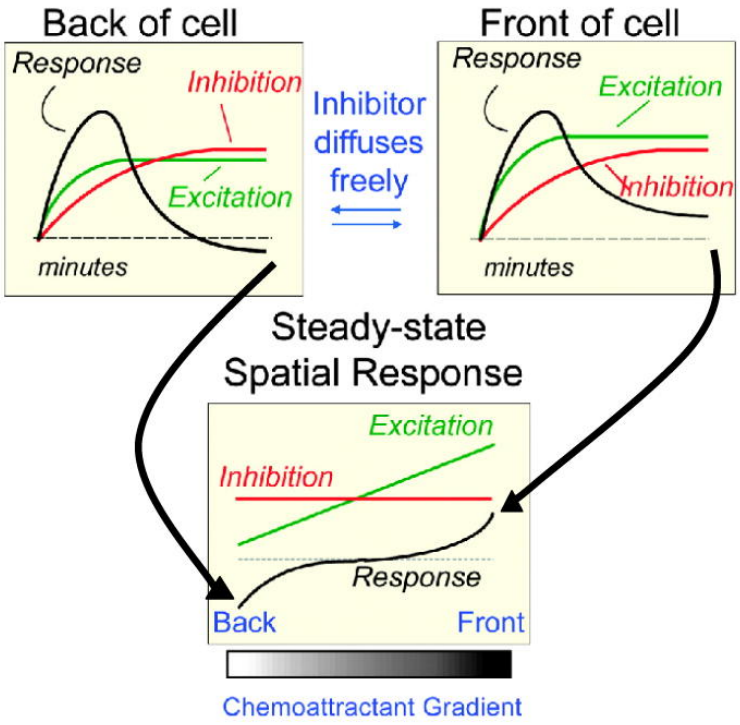

Figure 2. In a chemoattractant gradient, the response at the front and back of the cell is the difference between localized excitation and global inhibition. The steady-state spatial response polarizes the cell and steers migration.[8]

To respond to protein gradients, cells proceed through three steps: initial detection of a gradient, polarization with the gradient, and migration along the gradient (**Figure 1**).[3, 4, 8] While the full mechanism for gradient-driven chemotaxis is still being worked out, the most comprehensive model is the local excitation, global inhibition model (**Figure 2**).[8] In this model, cells detect a protein gradient through a uniform distribution of G protein-coupled receptors on their surface, which translate the chemoattractant gradient along the outer fold of the membrane into a gradient of excitatory signaling local to the inner fold. Slower inhibitory signals diffuse throughout the cell and determine a global threshold. At the lower end of the concentration gradient, excitatory signaling does

not rise above the inhibitory threshold and no cytoskeletal rearrangement occurs. However, the excitatory signaling at the higher end of the concentration gradient overcomes the threshold and spurs further downstream signaling that results in actin polymerization, cell polarization, and establishment of a leading edge for cell chemotaxis. As the cell migrates down the gradient, the leading edge of the cell continues to encounter ever-higher concentrations of chemoattractant, which continues to drive the cell along the chemoattractant gradient. When the gradient eventually plateaus or dips, the inhibitory signaling overcomes the excitatory and the cell arrests its movement [4, 8]. This model of chemotaxis demonstrates how protein gradients are able to inspire and direct cell behavior.

Attempts to simulate gradients have included the release and diffusion of factors from point sources or across microfluidic channels.[1, 2, 9-13] Unfortunately, gradients produced by point sources only last until the encapsulated protein is depleted and are limited in their extent of spatial patterning. Microfluidic devices have great versatility in producing different gradient patterns, but are confined to the *in vitro* setting without much potential for clinical translation. Another strategy, which produces persistent gradients and translates better to the clinical setting, is the patterning of gel (polydimethylsiloxane or polyethylene glycol) surfaces with proteins.[10, 14] While gels mimic the disorganized soft-tissue environment, many of the tissues within the body contain highly-organized ECM, such as tendon, muscle, nerve tissue, and blood vessels.[15-18] Combining a persistent gradient with an aligned polymer scaffold could improve the outcome of tissue engineering constructs by accelerating cell proliferation and infiltration.

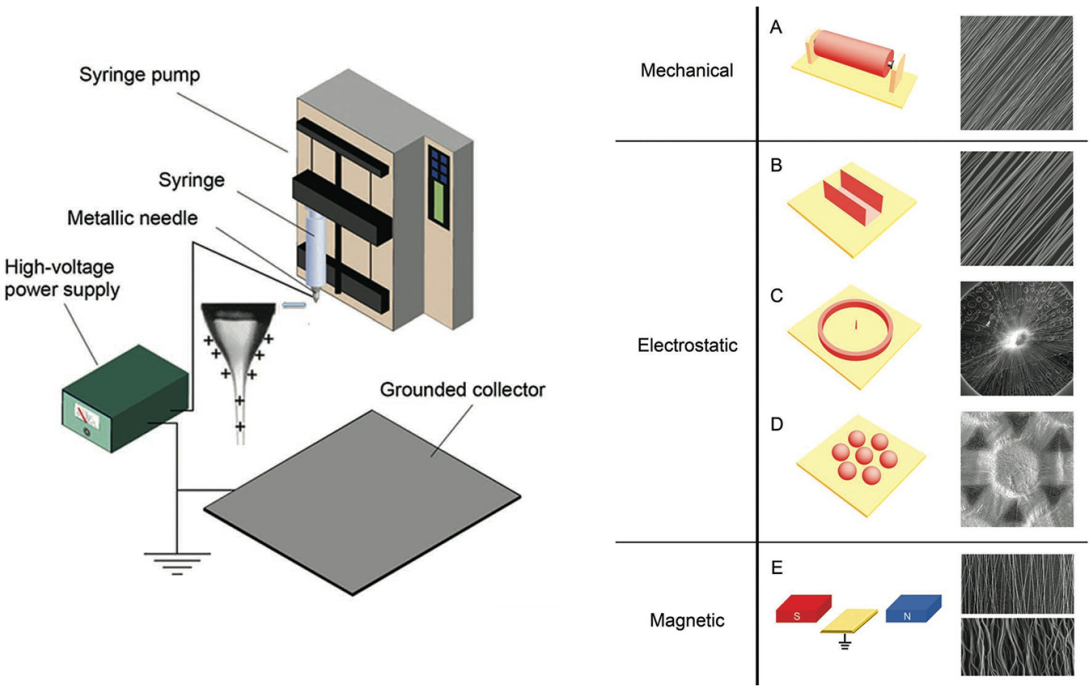

Figure 3. Electrospinning setup and various grounded collectors to produce different nanofiber scaffold architectures.[19]

1.2 Nanofibers in Tissue Engineering

Electrospinning is a technique used to produce polymer fiber scaffolds. To briefly describe the procedure for electrospinning: a polymer is dissolved in a volatile solvent mixture and pumped through a blunt metallic needle that has been connected to a high-voltage power supply. The high-voltage induces charges to collect on the surface of the polymer solution droplet and form the droplet into a Taylor cone. Polymer solution is ejected from the tip of the Taylor cone toward a grounded collector. As the polymer solution travels from the needle to the collector, the stream elongates, the solvent evaporates, and instabilities cause the stream to whip around so that dry polymer fibers are deposited on the collector (**Figure 3**). Depending on the electrospinning parameters, fibers with nanoscale diameters and high surface-area-to-volume ratios can be spun.

These nanofibers mimic the structure of fibers found in native ECM and can be spatially arranged to mimic the organization of the ECM of various tissues (**Figure 3**).[19]

One of the biggest challenges for employing nanofibers as tissue-engineering constructs is the incorporation of biochemical cues. Strategies have ranged from physical association (adsorption or ionic) and encapsulation to covalent immobilization.[20-23] The next step is adapting these approaches to produce gradients on modified nanofibers. From a thorough examination of the relevant literature, no successful attempts at creating a protein gradient on nanofibers through covalent immobilization have been published. However, Viswanathan et al. were able to control the extent of peptide presentation by varying the ratio at which two different block co-polymers were blended in their electrospinning solution.[24] Even if this strategy were adapted to produce a spatial protein or peptide gradient, the use of exotic block co-polymers limits its applications.

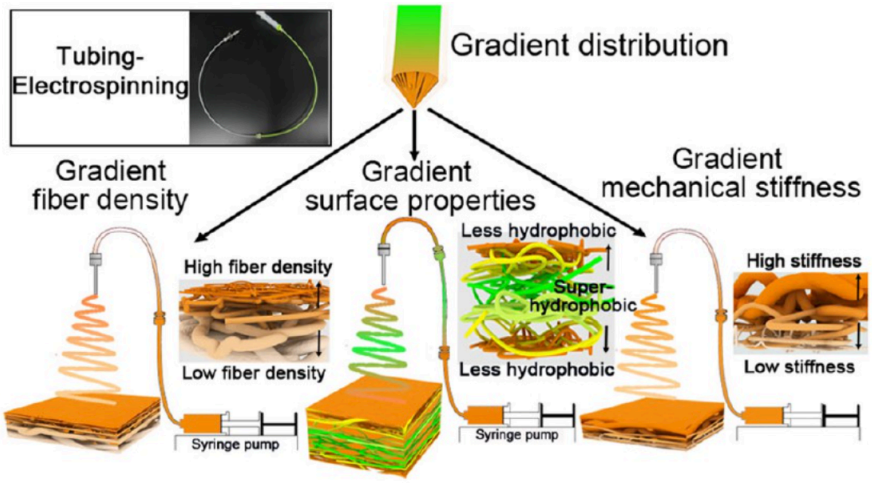

Figure 4. Z-gradients of nanofiber properties can be created by placing different polymer solutions in sequential tube sections prior to electrospinning.[25]

Kim et al. developed a method to produce a gradient of physical and/or chemical properties through the thickness of a nanofiber mat. Their approach consists of placing different polymer solutions along a length of tubing so that some mixing occurs at the interfaces between the solutions (**Figure 4**). Z-gradients of nanofiber density, hydrophobicity, or mechanical stiffness were successfully electrospun.[25] This method has the potential to be adapted to produce gradients in the XY-plane by moving the grounded collector during the electrospinning process. To produce gradients of protein, the methods of Viswanathan et al. and Kim et al. could potentially be combined.

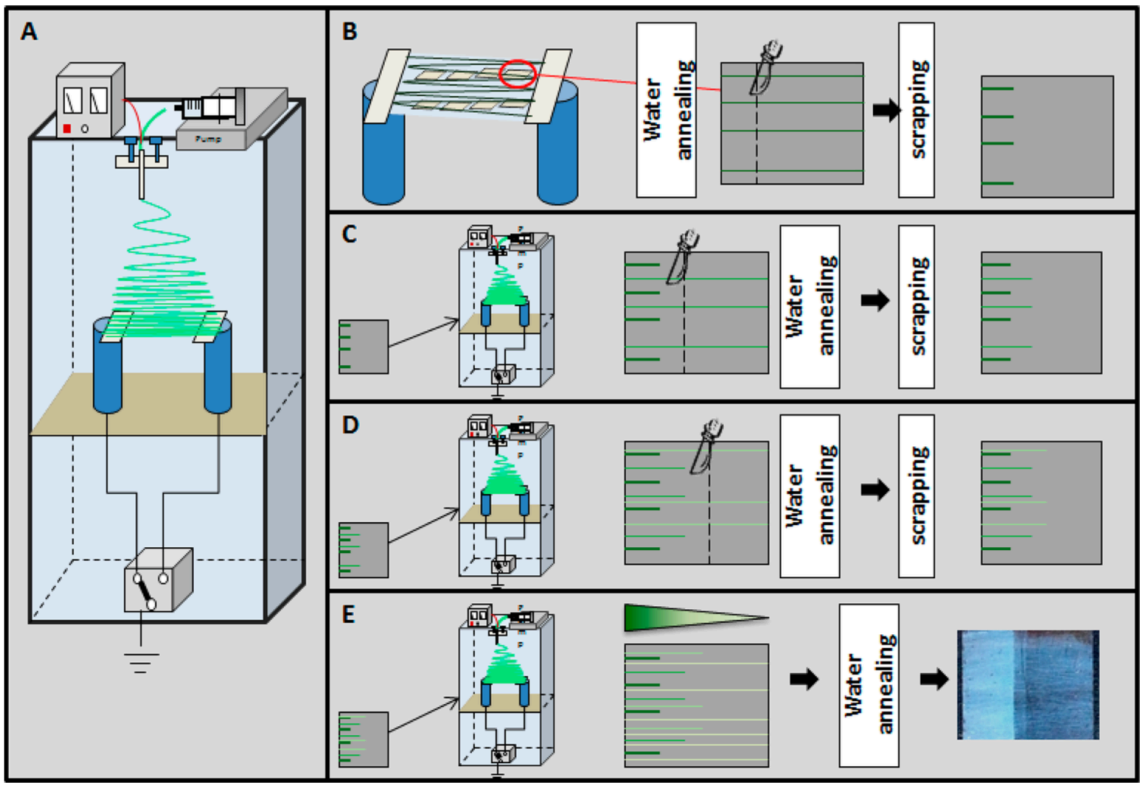

Figure 5. Aligned nanofibers loaded with varying amounts of NGF were sequentially electrospun and trimmed until a gradient of fiber density and encapsulated NGF was produced.[26]

Dinis et al. created a gradient of encapsulated NGF by electrospinning aligned nanofibers with a large amount of encapsulated protein and cutting away all but a small portion of the fibers (**Figure 5**). They repeated the process while successively reducing the amount of encapsulated NGF and the portion of fibers cut away until a full gradient was formed.[26] While the strategy allows control over the gradient profile and composition, the gradient is ultimately discrete and the changes in protein concentration would appear as large steps at the length-scale of a cell. Furthermore, a significant amount of NGF is wasted during the construction of the gradient by discarding NGF-loaded nanofibers at every step.

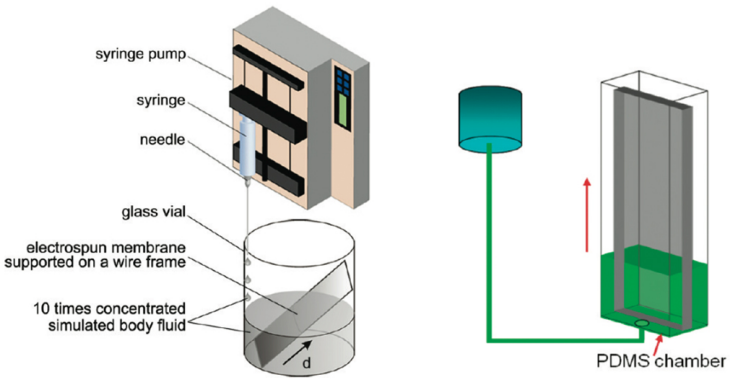

Figure 6. Two filling-up methods to produce gradients of mineral content or fibronectin.[27, 28]

Another approach was used to produce a gradient of mineral content along the length of a nanofiber mat for insertion at a tendon-to-bone interface. Li et al. placed a strip of nanofiber mat in an empty beaker and then pumped in a concentrated calcium solution (**Figure 6**).[27] The amount of mineralization was proportional to the duration the nanofibers were exposed to the concentrated calcium solution.[27, 29] Therefore, nanofibers at the bottom of the strip had greater mineral content than nanofibers at the top.[27] Shi et al. used the same approach to generate gradients of fibronectin on

polymethylglutarimide nanofibers. To limit the amount of protein solution needed, Shi et al. used a custom-made PDMS chamber that only required 0.5 mL of solution to completely fill (**Figure 6**).[28]

As can be seen from the various examples, there is much interest in developing protein gradients on nanofiber mats and many strategies are being developed towards that goal. Disadvantages with the current methods include the use of overly complicated methods, use of exotic materials, use of relatively large amounts of bioactive protein, or waste of bioactive protein. The most promising approach to creating a continuous gradient is the filling method.[27, 28] However, there are issues with the amount of bioactive protein needed and the overall versatility that still need to be addressed.

1.3 Objective

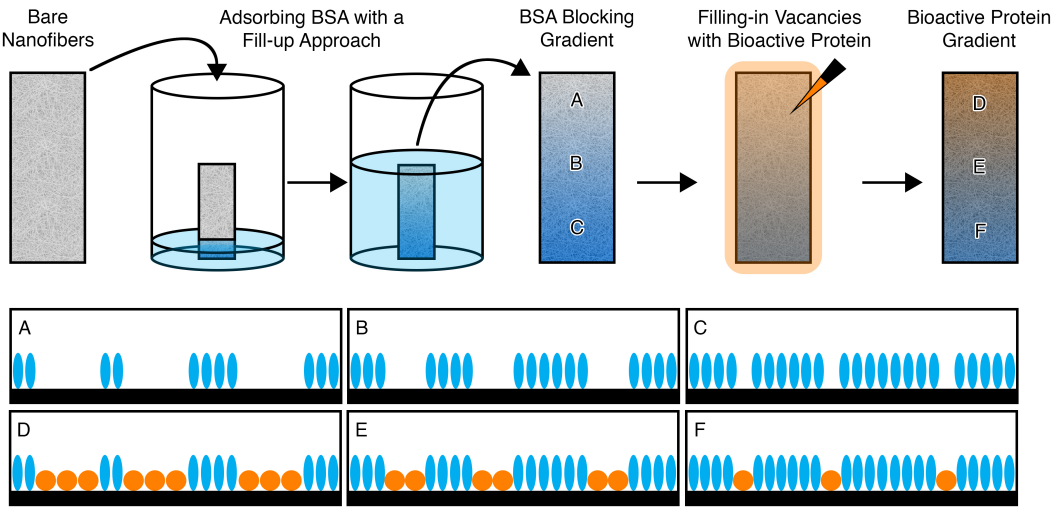

Figure 7. Schematic for generating a gradient of bioactive protein on a nanofiber scaffold. First, a gradient of inert BSA protein (A-C) is created on the plasma-treated nanofibers. Then, the vacancies left are filled in by a solution of bioactive protein to generate a gradient that runs countercurrent to the BSA gradient (D-F).

In this study, the strategy presented in **Figure 7** is employed to indirectly create a gradient of bioactive protein on a nanofiber mat. First, BSA is adsorbed onto nanofibers in a gradient to act as a mask by blocking off portions of the nanofibers. Then, a bioactive protein fills in the vacancies left by the BSA and produces a gradient that runs countercurrent to the BSA gradient. By creating a BSA mask instead of adsorbing the bioactive protein gradient directly, limited and expensive bioactive protein is not wasted in the considerable volume of solution needed to make the gradient. Instead, the relatively abundant and cheap BSA is exploited. Additionally, conditions required to produce the BSA gradient need only be found once for a given platform, rather than optimizing conditions for many different bioactive proteins. As a proof of concept for the possible applications towards regenerative medicine, a gradient of NGF on aligned PCL nanofibers was created and then embryonic chick DRG were seeded on the functionalized nanofibers to observe neurite extension along an adsorbed NGF gradient.

CHAPTER 2. MATERIALS AND METHODS

2.1 Materials

BSA, BSA-FITC, PCL (80,000 g/mol MW), formaldehyde, pyridine, formic acid, DMF, DCM, PBS (10x concentrated), Tween 20, and anti-neurofilament 200 were all purchased from Sigma-Aldrich (St. Louis, Missouri). Pyridine and formic acid were mixed in equimolar amounts to produce PF.[30] Silastic Type A Medical Adhesive was purchased from Dow Corning Co (Midland, MI, USA). HBSS, neural basal media, N-2 supplement, ABAM, and Alexa Fluor 488 goat anti-mouse IgG were all purchased from Invitrogen (Carlsbad, CA). NGF was purchased from R&D system (Minneapolis, MN).

2.2 Nanofiber synthesis and characterization

2.2.1 Electrospinning PCL nanofibers

Pellets of PCL were dissolved at 5% w/v in a solution of PF, DMF, and DCM at a volume ratio of 5:15:80 and sonicated in cold water for about 1 hour. The PCL solution was then loaded into a syringe with a 23-gauge needle and ejected from the syringe at a rate of 0.5 mL/hour using a syringe pump (KD Scientific, Holliston, MA). Aluminum foil, as the grounded collector, was placed 20.0 cm away from the needle tip and a voltage of 18 kV was applied between them (Gamma High Voltage Research, Ormond Beach, FL). The ambient atmospheric conditions were about 20 °C and 40% humidity. Electrospinning was terminated after 2.0 mL of PCL solution had been dispensed.

To produce aligned nanofibers for the DRG neurite extension studies, PCL was

dissolved at 12% w/v in a 1:4 DMF:DCM mixture. The solution was ejected from a syringe at a rate of 1.0 mL/hour with an accelerating voltage of 15 kV. A U-shaped steel collector was placed 20.0 cm away from the syringe tip and nanofibers were collected for 6 minutes (0.1 mL solution dispensed).

2.2.2 Nanofiber characterization

SEM images were obtained for nanofiber sections that had been subjected to varying plasma exposure durations (0, 0.5, 1, 2, or 5 minutes) or were soaked in solution (PBS, 0.1% BSA, or 0.5% BSA) for 1 hour. The sections were coated by a Hummer 6 Au/Pd sputter-coater (Anatech, Union City, CA) and imaged with a Hitachi 8230 Cold Field Emission SEM (Tokyo, Japan). The diameters of 100 nanofibers from each treatment were evaluated by ImageJ software. Statistical significance was evaluated using Student's T-test.

2.3 BSA adsorption on PCL nanofibers

2.3.1 Kinetics

Circular sections of 1-cm diameter were punched out from a PCL nanofiber mat, weighed, placed in 24-well plates, and exposed to plasma for 2 minutes (PlasmaEtch, Carson City, NV). BSA solutions of 0.1% or 0.5% w/v were prepared in 1x PBS and 1 mL was added to all of the wells. After 5, 10, 20, 30, 45, or 60 minutes, the BSA solutions were removed and the nanofiber sections were rinsed with PBS for three times to remove the unadsorbed free BSA. All time-points were repeated in triplicate. Then, 70 μL of 0.5% w/v BSA-FITC in PBS solution was placed on each nanofiber section and

kept in the dark at room temperature for 2 hours. Afterwards, the sections were washed in 0.1% v/v Tween 20 in diH_2O three times, rinsed in PBS three times, and sealed in glass slides. The sections were imaged using a Leica 6000 B inverted microscope (Buffalo Grove, IL) and GFP filter at 2.5x magnification.

The average fluorescent intensity of each nanofiber section was obtained using MATLAB and then normalized to the weight of the respective nanofiber section. After subtracting the initial, normalized fluorescence value (c_0; 0 minutes) from the respective 0.1% and 0.5% BSA sets, the data could be linearized by a Hanes-Woolf transform and so maximum BSA coverage (c_{max}) and time to half of maximum coverage (T_m) values were obtained and functions of the form of equation 1 were fit to the data.

$$c(t) = c_0 - \frac{c_{max}t}{T_m - t} \quad (1)$$

2.3.2 Modeling of BSA adsorption

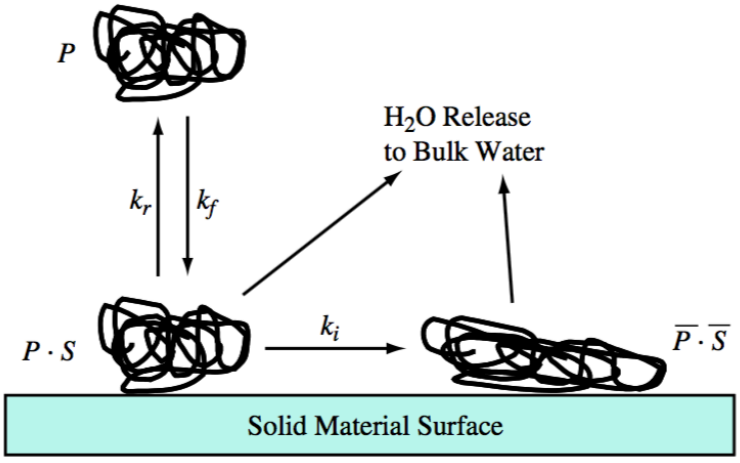

Figure 8. General model for protein adsorption.[31]

A general model for protein adsorption to a surface is shown in **Figure 8**. A protein in solution at concentration *P* (in mg/mL) reversibly binds to a surface *S* with on and off rates of k_f and k_r, respectively. The surface-interacting protein $P \cdot S$ can then rearrange its folding to become irreversibly bound to the surface $\overline{P \cdot S}$ at a rate of k_i. The rate equations describing the kinetics of this process are shown below:[31]

$$\frac{d[P \cdot S]}{dt} = k_f[P][S] - k_r[P \cdot S] - k_i[P \cdot S] \quad (2)$$

$$\frac{d[\overline{P \cdot S}]}{dt} = k_i[P \cdot S] \quad (3)$$

In order to find a solution to equations 2 and 3 that describes the amount of BSA adsorbed to the nanofiber mesh surface with respect to time, a few assumptions were made about the system. First, the amount of BSA in solution (represented by *P*) is in such excess that its concentration remains constant throughout the process. Secondly, the amount of remaining surface available for protein to adsorb to is represented by equation 4:

$$[S] = [S]_{total} - [P \cdot S] - [\overline{P \cdot S}] \quad (4)$$

Where $[S]_{total}$ is the total amount of surface available for protein adsorption at the very beginning of the process. Since all of the data from the BSA adsorption experiment was normalized to the weight of the nanofiber punch (which is directly proportional to the amount of surface area in the nanofiber mesh), it was ultimately assumed that $[S]_{total} = 1$. Rearranging equations 3 and 4, plugging them in to equation 2, and then simplifying the result yielded the ordinary differential equation 5:

$$\frac{d^2[\overline{P \cdot S}]}{dt^2} + \left(k_f P + k_r + k_i\right)\frac{d[\overline{P \cdot S}]}{dt} + k_f k_i P \cdot [\overline{P \cdot S}] = k_f k_i P \tag{5}$$

Characteristic and particular solutions were found for equation 5. Based on initial conditions where no adsorbed protein is present at the very beginning ($[\overline{P \cdot S}] = 0$ at $t = 0$) and, given enough time, the nanofiber surface becomes saturated with irreversibly bound protein ($\frac{d[\overline{P \cdot S}]}{dt} = 0$ as $t \to \infty$), the general solution to equation 5 becomes:

$$[\overline{P \cdot S}] = Ae^{m_1 t} - (A+1)e^{m_2 t} + 1 \tag{6}$$

Where

$$m_1 = \left(-\left(k_f P + k_r + k_i\right) + \sqrt{\left(k_f P\right)^2 + 2(k_r - k_i)k_f P + (k_r + k_i)^2}\right)/2 \tag{7}$$

$$m_2 = \left(-\left(k_f P + k_r + k_i\right) - \sqrt{\left(k_f P\right)^2 + 2(k_r - k_i)k_f P + (k_r + k_i)^2}\right)/2 \tag{8}$$

A is a constant whose value cannot be determined from equation 6 and the given initial conditions. However, by plugging equation 6 into equation 3 and applying the initial condition that no protein is in contact with the nanofiber surface at the very beginning ($[P \cdot S] = 0$ at $t = 0$), the value for *A* in terms of constants *P*, k_f, k_r, and k_i can be found:

$$A = {}^{m_2}/_{m_1 - m_2} \tag{9}$$

Finally, the time-courses for all species in the adsorption process in terms of constants *P*, k_f, k_r, and k_i can be found:

$$[\overline{P \cdot S}] = \left({}^{1}/_{m_1 - m_2}\right)(m_2 e^{m_1 t} - m_1 e^{m_2 t}) + 1 \tag{10}$$

$$[P \cdot S] = \left({k_f P}/{m_1 - m_2}\right)(e^{m_1 t} - e^{m_2 t}) \tag{11}$$

$$[S] = \left({1}/{m_1 - m_2}\right)\left(k_f P(e^{m_2 t} - e^{m_1 t}) - m_2 e^{m_1 t} + m_1 e^{m_2 t}\right) \tag{12}$$

To determine values for the rate constants, the data from the BSA adsorption experiments was normalized to the initial fluorescent intensity value after background fluorescence was subtracted out. Then, an array of values for each rate constant was tested from 0 to 10 with a step of 0.1 to find the combination of values that minimized the error between the model (equation 12) and the real data. Once the general area had been found, another array of values centered around the previous result ± 0.1 with a step of 0.001 was tested for a combination with better resolution.

2.3.3 Generating Gradients

Strips of nanofibers at least 40 mm long and 5 mm wide were cut out and mounted on glass slides with Silastic Type A Medical Adhesive. Starting and ending points (35 mm distance from each other) were marked on the glass slides and then the slides were exposed to plasma for 2 minutes. The nanofiber strips were placed vertically in an empty beaker and 0.1% BSA solution in PBS was placed in a separate beaker. The BSA solution was transferred between the beakers until the solution level was even with the starting point, then the solution was transferred at a rate of 3.0 mL/hour using an Easy-Load II peristaltic pump (Cole-Parmer, Vernon Hills, IL). After the solution level reached the ending point (about 1 hour later), the slides were removed from the BSA solution and immediately rinsed with PBS twice.

In order to visualize the generated gradients, 200 µL of 0.5% BSA-FITC in PBS

solution was placed along each nanofiber strip and incubated in the dark at room temperature for about 2 hours. Afterwards, the nanofiber strips were washed in 0.1% Tween 20 solution twice, rinsed in PBS twice, and sealed with a glass coverslip. The strips were imaged at three spots (both edges and in the middle of the strip) every 5 mm from the ending point (0 mm) to the starting point (35 mm) at 20x magnification. The average fluorescence intensity at each position was calculated in MATLAB and plotted.

To produce a gradient of NGF on nanofibers for the neurite extension study, aligned PCL nanofibers were affixed to glass coverslips (22 x 22 mm) and plasma-treated for 2 minutes. Then, two coverslips (oriented such that the fiber orientation ran vertically) were stood up in the well of a 6-well plate while 0.1% BSA in PBS solution was pumped in over 1 hour with a syringe pump. As controls, two sets of coverslips were immersed completely in 0.1% BSA solution or PBS for 1 hour. Afterwards, all coverslips were rinsed in PBS three times and sterilized under UV light for 1 hour. NGF (200 μL of 10 μg/mL solution) was placed on the nanofibers with a BSA gradient or that had been immersed in PBS only. As a control, PBS was placed on the nanofibers that had been completely immersed in BSA. All nanofibers were then incubated at 4 °C overnight before rinsing with PBS and seeding DRG.

2.4 Neurite extension study

2.4.1 Isolation and culture of DRG

All DRG were isolated from the thoracic region of the spinal column in embryonic chicks via sterile microdissection. Embryonic day 8 (E8, stage HH35-36) chicks were removed from the white leghorn eggs and decapitated. DRG were dissected

from the thoracic region and collected in HBSS. The DRG cells were then seeded onto the center of the nanofiber mats (1 DRG per sample) and subsequently cultured for 6 days in a modified neurobasal medium supplemented with 1% N-2 supplement and 1% ABAM. As a positive control, some DRG were cultured in media supplemented with 50 ng/mL NGF.

2.4.2 Immunostaining of DRG

After culturing for 6 days, the DRG neurons were immunostained with anti-neurofilament 200. Briefly, the samples were fixed in 3.7% formaldehyde at room temperature for 45 minutes, blocked with PBS containing 3% BSA for 1 hour, and then incubated with anti-neurofilament 200 diluted (1:500) in PBS containing 0.1% BSA overnight at 4 ^{o}C. The anti-neurofilament 200 marker was detected using Alexa Fluor 488 goat anti-mouse IgG (1:200) secondary antibody at room temperature for 1 hour. Between each procedure, the samples were washed three times in PBS. After staining, fluorescence micrographs were captured using a laser confocal scanning microscope (Zeiss LSM 700). The average lengths of extending neurites on either side of the DRG mass were calculated from fluorescence images by choosing 10 neurites from each side and measuring their length in ImageJ. Statistical analysis was performed using Student's T-test by analysis of variance at a 95% confidence level.

CHAPTER 3. RESULTS AND DISCUSSION

3.1 Nanofiber characterization

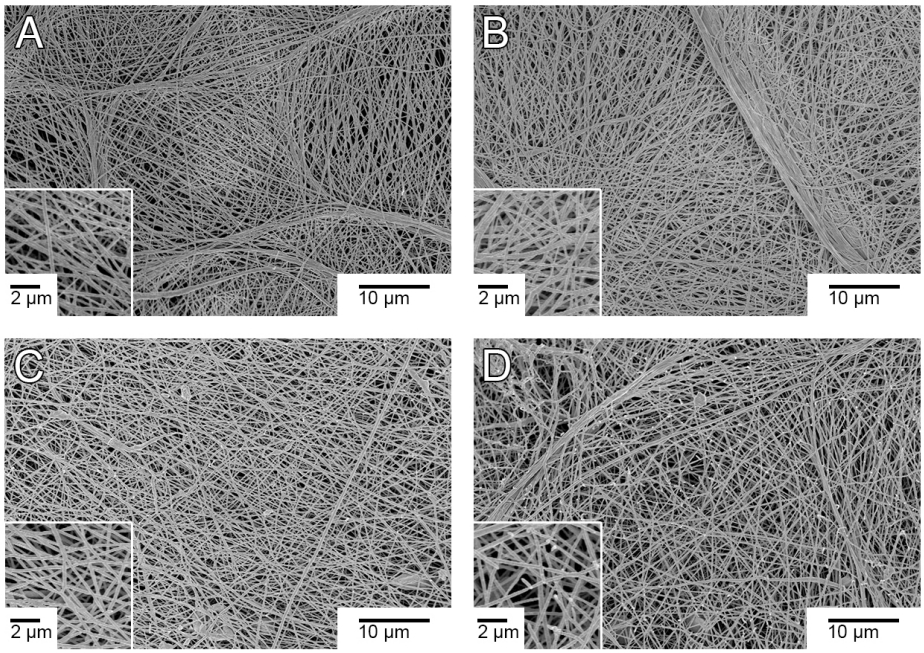

Figure 9. Plasma treatment of random PCL nanofiber mats for (**A**) 30 seconds, (**B**) 1 minute, (**C**) 2 minutes, or (**D**) 5 minutes.

Exposure to plasma introduces carboxyl and hydroxyl groups onto the surface of the PCL nanofibers, which imparts hydrophilicity on the initially hydrophobic nanofibers.[20, 28] This hydrophilicity is necessary not only for cell attachment and growth on nanofibers, but also for successful aqueous treatments and modifications.[20, 28] **Figure 9** shows the SEM images of the nanofiber mats after being exposed to plasma for different times. When compared to pristine PCL nanofibers (**Figure 10A**), no discernable changes in nanofiber morphology were found after the nanofibers were

exposed to plasma for 30 seconds, 1 minute, and 2 minutes. However, after 5 minutes of plasma exposure, the nanofibers began to melt and rupture. So all nanofiber samples discussed in the present work were exposed to plasma for 2 minutes from this point forward.

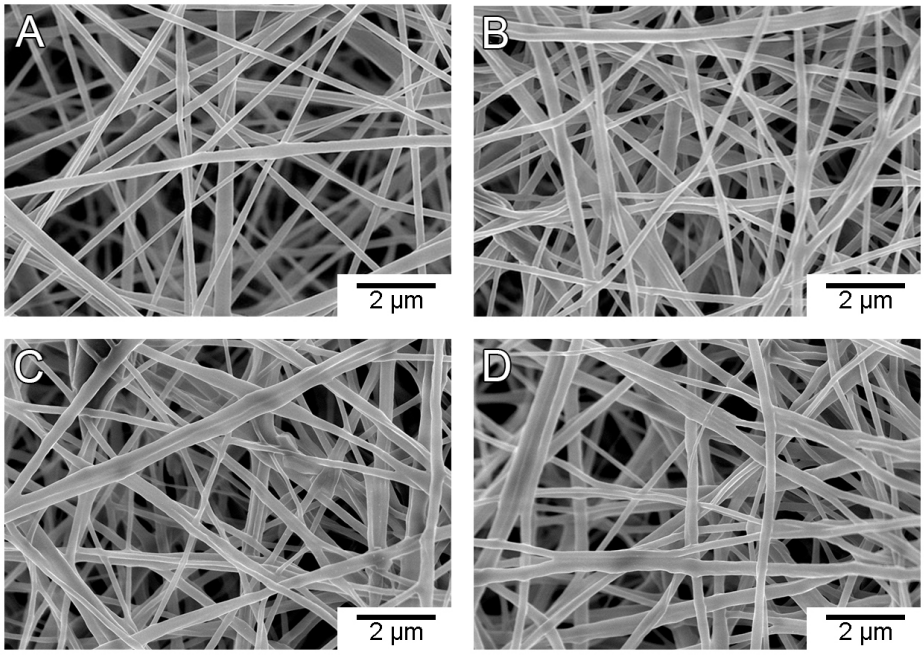

Figure 10. SEM images of (**A**) pristine nanofibers or nanofibers that had been plasma-treated for 2 minutes and soaked in (**B**) PBS, (**C**) 0.1% BSA solution, or (**D**) 0.5% BSA solution for 1 hour.

After plasma exposure, PCL nanofiber sections were immersed in PBS, 0.1% BSA, or 0.5% BSA solution for 1 hour. SEM images of the nanofiber sections are shown in **Figures 10 and 11**. Compared to the pristine nanofibers, the treated nanofibers exhibited no change in morphology or texture. However, plasma treatment and subsequent immersion in PBS caused the nanofibers to swell from an average diameter of 210 ± 7 nm to 243 ± 7 nm (**Table 1**). The adsorption of BSA to the nanofibers further

increased the average diameter to 257 ± 9 nm or 264 ± 8 nm after the nanofibers were immersed in 0.1% or 0.5% BSA solution, respectively. The difference in diameter between the BSA-soaked and PBS-soaked nanofibers (14 nm or 21 nm) is less than twice the size of the long axis of the BSA protein, which is modeled as an ellipsoid with two short axes of length 4 nm and a long axis of length 14 nm.[32] According to previous literature, proteins spread across a surface during adsorption and only adsorb in monolayers.[31, 33] In the more-concentrated 0.5% BSA solution, the rate of adsorption is greater than that of the 0.1% solution and, therefore, the BSA proteins pack tighter with less spreading, which would explain the discrepancy in diameters of the two BSA-exposed nanofiber samples.[33]

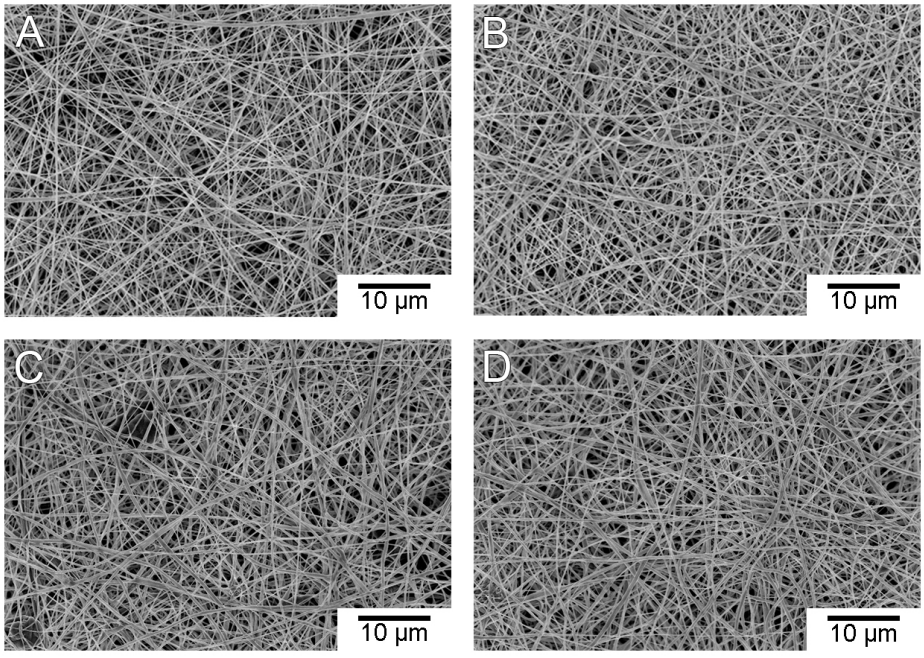

Figure 11. SEM images of PCL nanofibers used to calculate the average diameter for (**A**) pristine nanofibers or nanofibers that had been soaked in (**B**) PBS, (**C**) 0.1% BSA solution, or (**D**) 0.5% BSA solution for 1 hour after a 2-minute plasma-treatment.

Table 1. Average diameter of nanofibers after various treatments.

Treatment	Pristine	PBS	0.1% BSA	0.5% BSA
Average Diameter (nm)	210 ± 7	243 ± 7	257 ± 9	264 ± 8

3.2 BSA adsorption kinetics

BSA adsorption onto PCL nanofibers is a time- and concentration-dependent process (**Figure 12**). The adsorption of BSA from a 0.1% solution demonstrates that the amount of adsorbed BSA increases with time. When comparing adsorption behavior from a 0.1% to a 0.5% BSA solution, the rate of BSA adsorption increases with solution concentration. Furthermore, there is a point of saturation at which adsorbed BSA occupies all of the available space on the nanofibers.

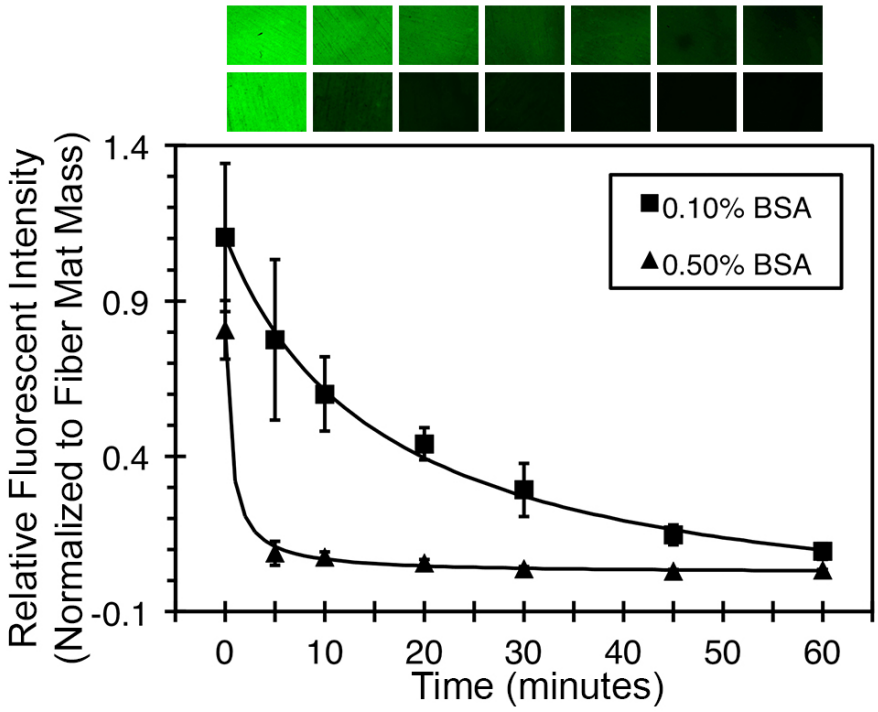

Figure 12. BSA adsorption on PCL nanofibers is dependent on the duration of exposure to BSA solution and the concentration of BSA (n=3 for each time point). Representative fluorescent images are included above the graph.

The relative fluorescent intensities of each time-point were subtracted from the relative fluorescent intensity of the sections that were not exposed to BSA (**Figure 13A**). This loss of fluorescent intensity represents the actual amount of BSA adsorbed over time rather than the amount of free space left, which the BSA-FITC represents. The loss of fluorescence data can be linearized by a Hanes-Woolf transform, which describes a saturation coverage (c_{max}) and a time to achieve half of the saturation coverage (T_m) (**Figure 13B**). For both the 0.1% and 0.5% BSA solution, the c_{max} values are similar (1.15 and 0.97, respectively) and indicate both solutions can saturate the PCL nanofibers to the same degree. However, the T_m values are vastly different (15.85 minutes and 0.61

minutes, respectively) and support the observation that the rate of BSA adsorption is higher for the more-concentrated 0.5% BSA solution. We chose to make gradients with the 0.1% BSA solution because the T_m is too short to make a gradient with the 0.5% BSA solution. At a 0.5% concentration, BSA would almost immediately adsorb to the nanofibers and limit the amount of nanofiber surface area left vacant for the bioactive protein to adsorb.

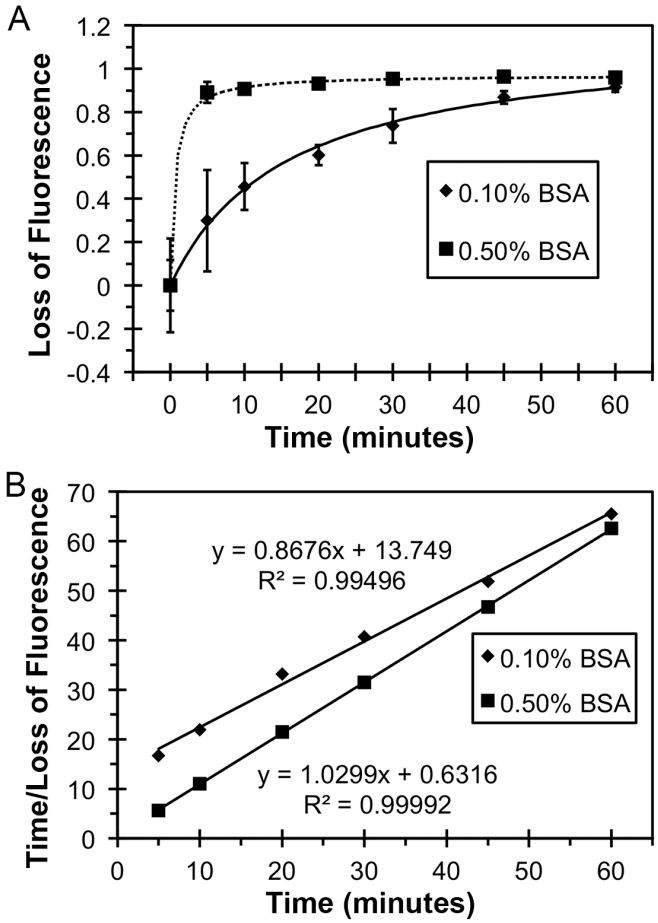

Figure 13. (**A**) Plotting the loss of fluorescence over time better represents the actual time course of BSA adsorption. (**B**) The loss of fluorescence data can then be linearized by a Hanes-Woolf transform and fit with a straight line, which can be used to determine a saturation point (c_{max}) and the time to half saturation (T_m).

3.3 Modeling BSA adsorption kinetics

The fluorescent intensity data from the BSA adsorption experiment represents the amount of surface area left on the nanofiber meshes for further protein adsorption. When equations 7, 8, and 12 were fit to the data, the rate constants for each process in the protein adsorption model from **Figure 8** were found and are shown in **Table 2**.

Table 2. Rate constants for BSA adsorption model

Rate Constant	$\mathbf{k_f}$ $(\mathbf{mL/mg{\cdot}s})$	$\mathbf{k_r}$ $(\mathbf{1/s})$	$\mathbf{k_i}$ $(\mathbf{1/s})$
Value	0.092	0.065	0.078

The first-order rate constants of k_r and k_i are of the same magnitude, but the process for a protein becoming irreversibly bound is slightly faster than for a protein to desorb from the surface. The second-order rate constant of k_f is also of a similar magnitude, but only when the BSA solution concentration is 1 mg/mL because the effective rate at which BSA initially interacts with the nanofiber surface is $k_f P$. So that when the BSA solution concentration is 5 mg/mL, we see that the surface quickly becomes saturated with BSA protein since the effective rate would be 0.46/s, which is a magnitude greater than the rate at which BSA would be removed from the surface.

The model shows excellent agreement with the BSA adsorption data (**Figure 14**), which allows us to predict how BSA will adsorb at other solution concentrations (**Figure 15**). The model could also be applied to determine how to create a BSA gradient in cases where a nanofiber mat is not on a flat, linear surface. For example, nanofibers could be

draped over a dome with a parabolic profile to create a radial gradient. The rate at which a BSA solution moves up the dome is not linear so the gradient profile would not appear the same as in **Figure 14**. But with the model, a BSA solution concentration and total immersion time could be selected to produce the desired gradient profile.

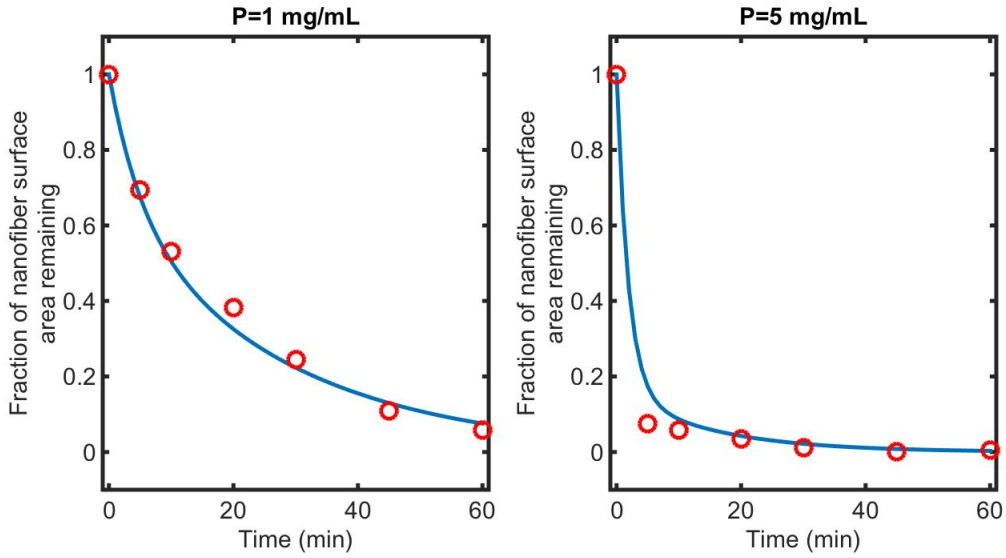

Figure 14. The model could reliably predict the fraction of nanofiber surface area remaining during the adsorption process.

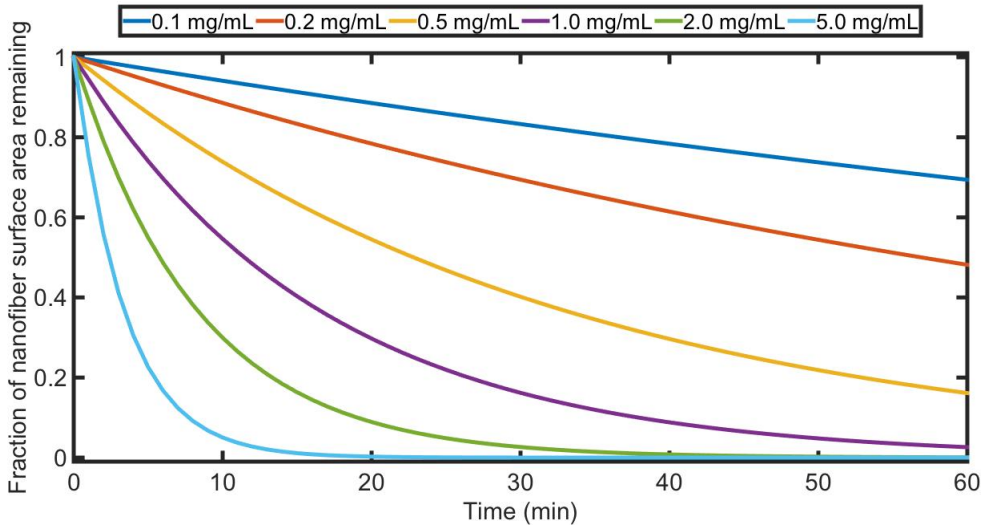

Figure 15. BSA adsorption time-courses predicted for varying concentrations of BSA solutions.

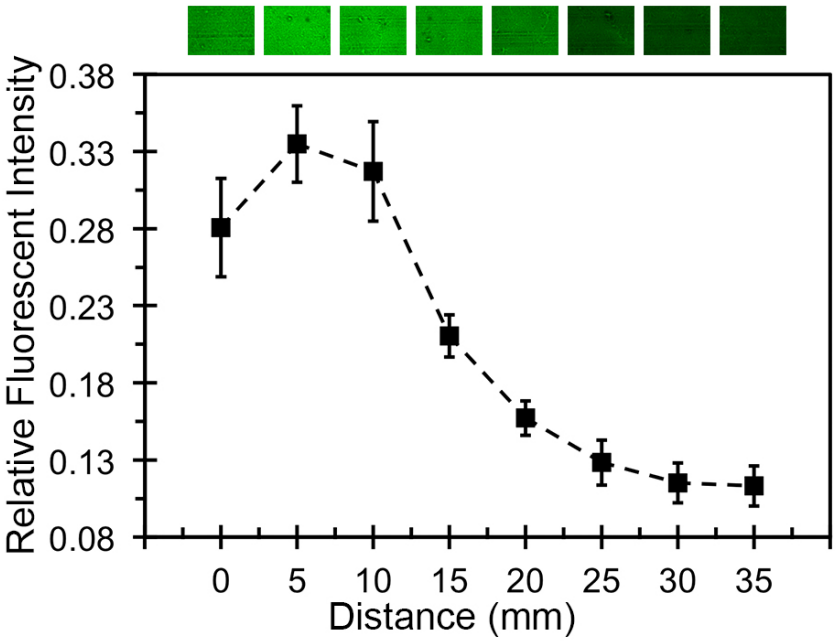

Figure 16. BSA adsorbed as a gradient on a strip of a nanofiber mat (n=9 at each position). Representative fluorescent images are included above the graph.

3.4 Generating a BSA gradient

Because the adsorption of BSA to PCL nanofibers is time dependent, a gradient can be created along a length of nanofibers by varying the amount of time a BSA solution is in contact with the nanofibers (**Figure 7**). In this work, we controlled the extent of BSA exposure by placing strips of nanofibers vertically in a beaker and filling the beaker up with 0.1% BSA solution at a constant rate. With this approach, the nanofibers at the bottom of the strip were exposed to BSA solution for a longer time than those at the top, and as a result, more BSA adsorbed to the bottom. We used BSA-FITC to fill in the vacancies left by the non-conjugated BSA and to visualize how a bioactive protein gradient might appear. **Figure 16** shows the visualized protein gradient generated along

three different strips with the same experimental conditions. The BSA gradient on both edges and down the middle proved to be similar among the different strips, which demonstrated the robustness of this gradient-generating strategy. Since the gradients were developed over the course of 1 hour in a 0.1% BSA solution, it is no surprise the profile of the gradient on the nanofiber strips (**Figure 16**) is similar to that of the adsorption time course (**Figure 12**). Unfortunately, the BSA gradient profile does not follow the BSA adsorption time course exactly. Instead, there is a significant drop in fluorescent intensity at the 0-mm mark. As shown in **Figure 17**, a dark area appears at the spot where the BSA solution stops during gradient creation. This boundary discrepancy could be the result of capillary action pulling up BSA solution since the marking is reminiscent of those seen in thin-layer chromatography. Perhaps increasing the rate at which BSA solution fills the beaker (which would also necessitate an increase in BSA concentration) to match the speed of the capillary front would fix the boundary discrepancy. Ultimately, we were able to generate a preliminary BSA masking gradient on the PCL nanofibers, after which different kinds of bioactive proteins could be adsorbed on the free sites of the nanofibers to generate a countercurrent gradient. Next, we used NGF as a model growth factor to demonstrate the influence a growth factor gradient would have on DRG neurite extension.

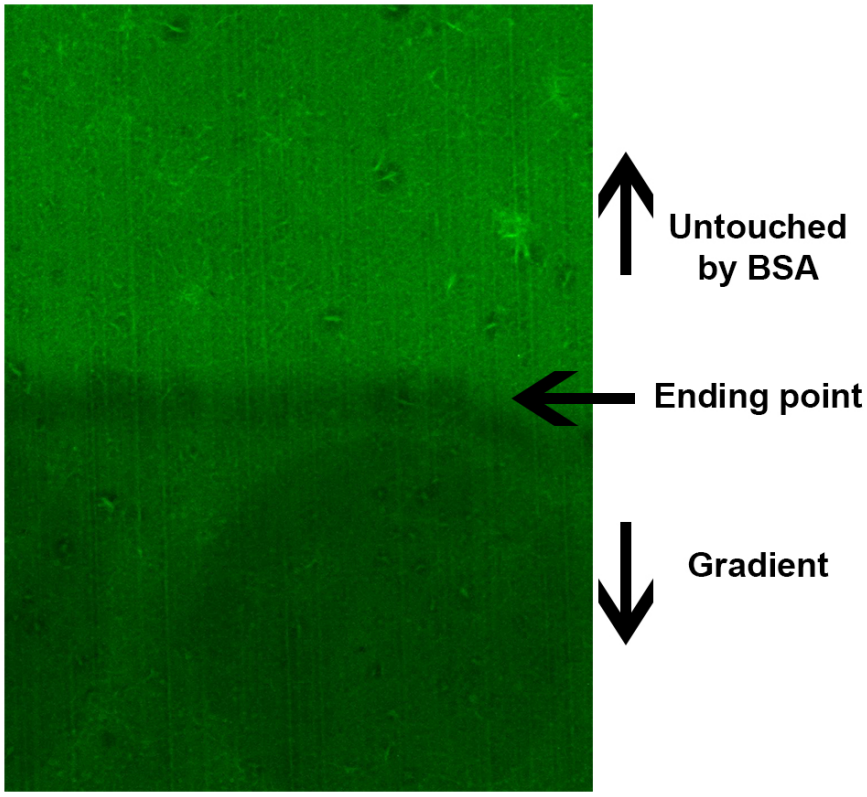

Figure 17. An increase in BSA adsorption occurs where the filling-up of BSA solution was stopped during the generation of a gradient.

3.5 DRG neurite extension

Aligned nanofibers have previously been shown to guide neurite extension.[17, 34] We attempt to take this a step further to guide and encourage neurite extension by generating an NGF gradient along the same direction as the aligned nanofibers. **Figure 18** shows the high-degree of alignment of the nanofibers through SEM. With the same procedure as described above, BSA was adsorbed to the aligned nanofibers as a masking gradient, then NGF was adsorbed on the BSA-blocked nanofibers to create an NGF gradient.

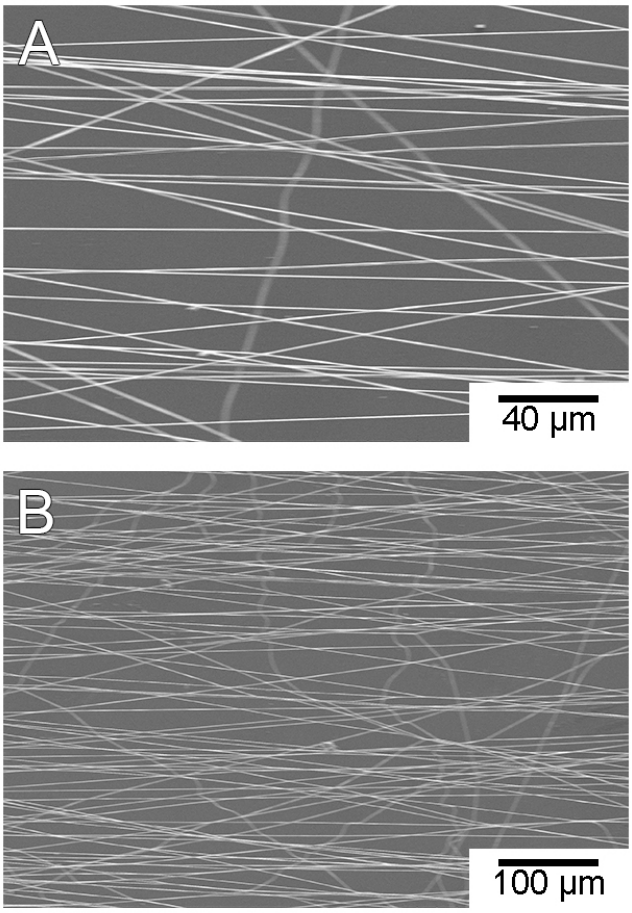

Figure 18. Aligned PCL nanofibers were used for the neurite extension study and were fabricated by electrospinning over a U-shaped piece of stainless steel.

Chick DRG cells were then seeded on aligned PCL nanofibers adsorbed with either a homogeneous or gradient distribution of NGF and cultured for 6 days. **Figure 19** shows the fluorescent images of the stained neurites extending from the DRG cell mass. The average neurite length extending from each side of the DRG mass was evaluated from the images and is shown in **Figure 20**. **Figure 21** shows the neurite extension of BSA-blocked aligned PCL nanofibers and the respective average neurite length. In all cases, axons extending out from the DRG cell mass followed the alignment of the PCL

nanofibers because of the contact guidance of the underlying nanofibers, which corroborates previous results.[17, 34]

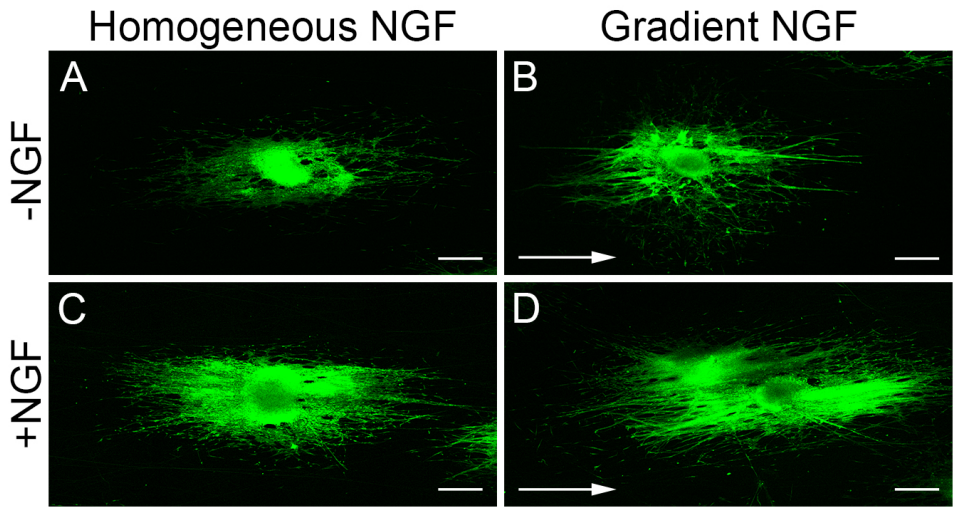

Figure 19. Chick DRG seeded on aligned PCL nanofibers with NGF (**A**, **C**) homogeneously adsorbed or (**B**, **D**) adsorbed as a gradient. (**C**, **D**) NGF was included in the culture media to further stimulate neurite extension. Scale bars are 500 μm in length.

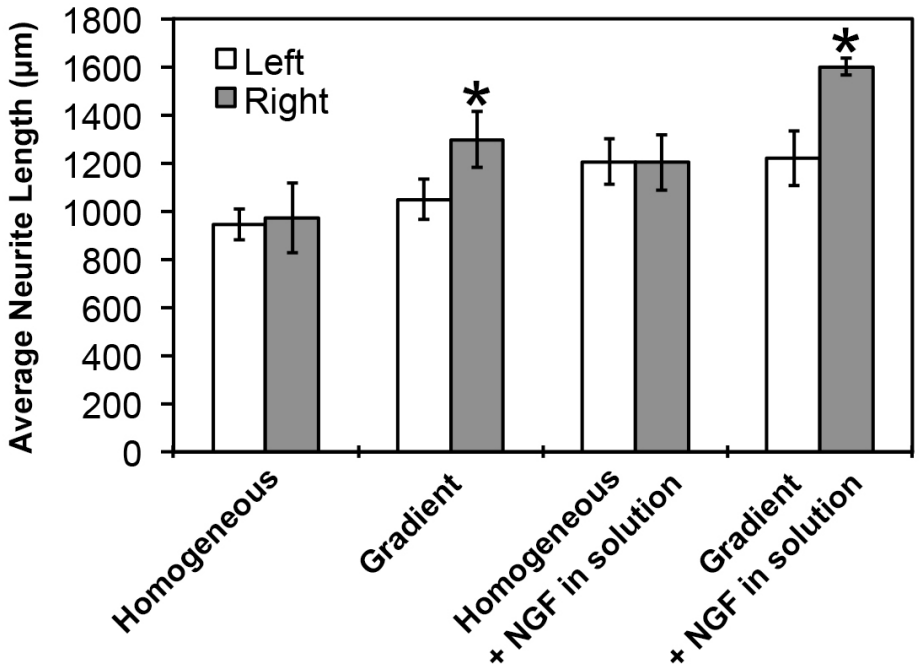

Figure 20. Average extension of neurites from DRG cell masses. Neurite extension along an NGF gradient (right) was significantly greater than extension against the gradient (left), while extension was even on both sides of the DRG when NGF was adsorbed homogeneously. (n=10; *p-value<0.05).

Addition of free NGF to the cell media slightly increased the average neurite length regardless of the nature of the adsorbed protein. When NGF or BSA was adsorbed homogeneously on the nanofibers, axons extended equally on either side of the DRG cell mass. When NGF was adsorbed as a gradient (increasing from left to right in **Figure 19** as the arrow directs), axons on the right side of the DRG cell mass extended significantly farther than axons on the left side. For the DRG grown on the nanofibers with adsorbed NGF gradient and soluble NGF in the medium, the neurite length on the right side of the DRG was almost 40% higher than that on the left side of the DRG. DRG neurites were

guided by the adsorbed NGF concentration gradient relative to control samples that have a homogeneous NGF concentration. The NGF gradient increased from left to right so axons to the right of DRG mass extended with the gradient while axons to the left extended against the gradient. On the nanofibers with adsorbed NGF, the growth cone of the DRG neurite recognizes the growth factor, expands its membrane, and then reaches for the next bound factor.[35] NGF increased the adherence of growth cones to the substrate, which benefitted the neurite extension by providing an anchor to further expand the growth cone. By increasing the NGF concentration along the nanofibers, the cell neurite growth cone could sense more growth factor within its reach and thus further expand its membrane along the direction of the gradient.[36] Besides, the DRG cells cultured on NGF-adsorbed nanofibers (**Figure 19**) had thickened neurites compared with those cultured on BSA-adsorbed nanofibers (**Figure 21**).

Curiously, the axons extending against the NGF gradient were not significantly shorter than the axons from the uniform NGF condition. The countercurrent BSA gradient might provide enough of a stimulus to the extending axons to partially overcome moving against the NGF gradient. In future studies, truly inert species such as PEG might serve as a better blocking material.

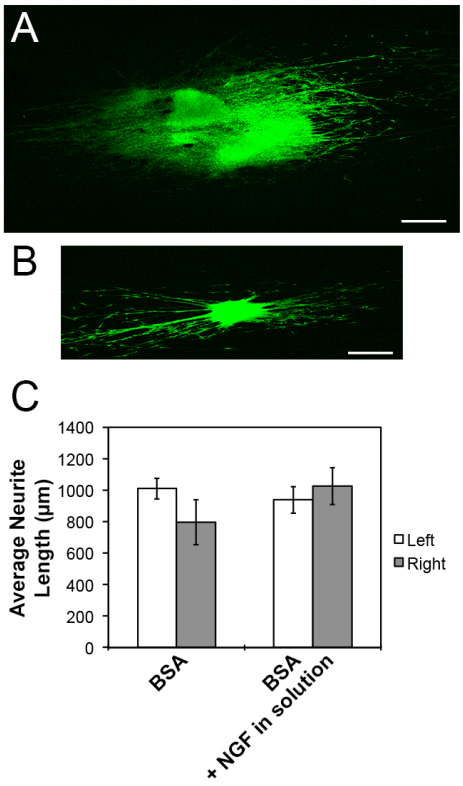

Figure 21. Neurite extension on BSA-adsorbed aligned nanofibers (**A**) without or (**B**) with NGF in the culture media. (**C**) There was no significant difference in neurite extension on either side of the DRG cell mass. Scale bars are 500 µm in length.

CHAPTER 4. CONCLUSIONS AND FUTURE WORK

In this study, the time-dependent adsorption of BSA to PCL nanofibers was employed to create an inert protein gradient. The vacancies left by the BSA gradient could then be filled-in by a bioactive protein to produce a countercurrent gradient. The described technique is a powerful strategy for creating gradients on nanofibers because it can be easily adapted to other nanofiber polymer systems and it conserves the amount of bioactive protein used. Bioactive proteins such as growth factors are often expensive and limited in quantity. By using an abundant, inert protein to construct a masking gradient, only small amounts of the bioactive protein were needed to produce a gradient. Furthermore, once the BSA adsorption profile is acquired for a given polymer nanofiber mat, any bioactive protein can fill in the vacancies and produce a gradient. We tested the effects an NGF gradient would have on neurite extension from a DRG cell mass and found axons extending with the gradient grew longer than axons extending against the gradient. With this initial success, future studies should be conducted with different bioactive proteins, different cell types, and different nanofiber architectures. For example, by draping some radially-aligned nanofibers over a dome and generating a radial BSA-blocking gradient, a patch for skin regeneration in diabetic ulcers could be constructed if the radial gradient were filled in with epidermal growth factor.

REFERENCES

1. Tucker, K. L., Meyer, M., and Barde, Y., Neurotrophins are required for nerve growth during development, *Nat. Neurosci.*, 2001, **4**, 29-37.
2. Gundersen, R. W. and Barrett, J. N., Neuronal chemotaxis: chick dorsal-root axons turn toward high concentrations of nerve growth factor, *Science*, 1979, **206**, 1079-1080.
3. Junger, W. G., Immune cell regulation by autocrine purinergic signaling, *Nat. Rev. Immunol.*, 2011, **11**, 201-212.
4. Iijima, M. and Devreotes, P., Tumor suppressor PTEN mediates sensing of chemoattractant gradients, *Cell*, 2002, **109**, 599-610.
5. Liu, L., Ratner, B. D., Sage, E. H., and Jiang, S., Endothelial cell migration on surface-density gradients of fibronectin, VEGF, or both proteins, *Langmuir*, 2007, **23**, 11168-11173.
6. Gunawan, R. C., Silvestre, J., Gaskins, H. R., Kenis, P. J. A., and Leckband, D. E., Cell migration and polarity on microfabricated gradient of extracellular matrix proteins, *Langmuir*, 2006, **22**, 4250-4258.
7. Arnold, M., Hirschfeld-Warneken, V. C., Lohmüller, T., Heil, P., Blümmel, J., Cavalcanti-Adam, E. A., López-García, M., Walther, P., Kessler, H., Geiger, B., and Spatz, J. P., Induction of cell polarization and migration by a gradient of nanoscale variations in adhesive ligand spacing, *Nano Lett.*, 2008, **8**, 2063-2069.
8. Janetopoulos, C. and Firtel, R. A., Directional sensing during chemotaxis, *FEBS Lett.*, 2008, **582**, 2075-2085.

9. Dertinger, S. K. W., Jiang, X., Li, Z., Murthy, V. N., and Whitesides, G. M., Gradients of substrate-bound laminin orient axonal specification of neurons, *Proc. Natl. Acad. Sci. U. S. A.*, 2002, **99**, 12542-12547.

10. Chung, B. G., Flanagan, L. A., Rhee, S. W., Schwartz, P. H., Lee, A. P., Monuki, E. S., and Jeon, N. L., Human neural stem cell growth and differentiation in a gradient-generating microfluidic device, *Lab Chip*, 2005, **5**, 401-406.

11. Millet, L. J., Stewart, M. E., Nuzzo, R. G., and Gillette, M. U., Guiding neuron development with planar surface gradients of substrate cues deposited using microfluidic devices, *Lab Chip*, 2010, **10**, 1525-1535.

12. Wang, Y. and Irvine, D. J., Engineering chemoattractant gradients using chemokine-releasing polysaccharide microspheres, *Biomaterials*, 2011, **32**, 4903-4913.

13. Zhao, X., Jain, S., Larman, H. B., Gonzalez, S., and Irvine, D. J., Directed cell migration via chemoattractants released from degradable microspheres, *Biomaterials*, 2005, **26**, 5048-5063.

14. DeLong, S. A., Moon, J. J., and West, J. L., Covalently immobilized gradients of bFGF on hydrogel scaffolds for directed cell migration, *Biomaterials*, 2005, **26**, 3227-3234.

15. Xie, J., Li, X., Lipner, J., Manning, C. N., Schwartz, A. G., Thomopoulos, S., and Xia, Y., Aligned-to-random nanofiber scaffolds for mimicking the structure of the tendon-to-bone insertion site, *Nanoscale*, 2010, **2**, 923-926.

16. Gillies, A. R., Bushong, E. A., Deerinck, T. J., Ellisman, M. H., and Lieber, R. L., Three-dimensional reconstruction of skeletal muscle extracellular matrix ultrastructure, *Microsc. Microanal.*, 2014, **20**, 1835-1840.

17. Xie, J., MacEwan, M. R., Li, X., Sakiyama-Elbert, S. E., and Xia, Y., Neurite outgrowth on nanofiber scaffolds with different orders, structures, and surface properties, *ACS Nano*, 2009, **3**, 1151-1159.

18. Wagenseil, J. E. and Mecham, R. P., Vascular extracellular matrix and arterial mechanics, *Physiol. Rev.*, 2009, **89**, 957-989.

19. Liu, W., Thomopoulos, S., and Xia, Y., Electrospun nanofibers for regenerative medicine, *Adv. Healthcare Mater.*, 2012, **1**, 10-25.

20. Yoo, H. S., Kim, T. G., and Park, T. G., Surface-functionalized electrospun nanofibers for tissue engineering and drug delivery, *Adv. Drug Delivery Rev.*, 2009, **61**, 1033-1042.

21. Jordan, A. M., Viswanath, V., Kim, S., Pokorski, J. K., and Korley, L. T. J., Processing and surface modification of polymer nanofibers for biological scaffolds: a review, *J. Mater. Chem. B*, 2016, **4**, 5958-5974.

22. Zheng, W., Wang, Z., Song, L., Zhao, Q., Zhang, J., Li, D., Wang, S., Han, J., Zheng, X., Yang, Z., and Kong, D., Endothelialization and patency of RGD-functionalized vascular grafts in a rabbit carotid artery model, *Biomaterials*, 2012, **33**, 2880-2891.

23. Kim, T. G. and Park, T. G., Biomimicking extracellular matrix: cell adhesive RGD peptide modified electrospun poly(D,L-lactic-co-glycolic acid) nanofiber mesh, *Tissue Engineering*, 2006, **12**, 221-233.

24. Viswanathan, P., Themistou, E., Ngamkham, K., Reilly, G. C., Armes, S. P., and Battaglia, G., Controlling surface topology and functionality of electrospun fibers on the nanoscale using amphiphilic block copolymers to direct mesenchymal progenitor cell adhesion, *Biomacromolecules*, 2015, **16**, 66-75.

25. Kim, J., Im, B. G., Jin, G., and Jang, J., Tubing-electrospinning: a one-step process for fabricating fibrous matrices with spatial, chemical, and mechanical gradients, *ACS Appl. Mater. Interfaces*, 2016, **8**, 22721-22731.

26. Dinis, T. M., Elia, R., Vidal, G., Auffret, A., Kaplan, D. L., and Egles, C., Method to form a fiber/growth factor dual-gradient along electrospun silk for nerve regeneration, *ACS Appl. Mater. Interfaces*, 2014, **6**, 16817-16826.

27. Li, X., Xie, J., Lipner, J., Yuan, X., Thomopoulos, S., and Xia, Y., Nanofiber scaffolds with gradations in mineral content for mimicking the tendon-to-bone insertion site, *Nano Lett.*, 2009, **9**, 2763-2768.

28. Shi, J., Wang, L., Zhang, F., Li, H., Lei, L., Liu, L., and Chen, Y., Incorporating protein gradient into electrospun nanofibers as scaffolds for tissue engineering, *ACS Appl. Mater. Interfaces*, 2010, **2**, 1025-1030.

29. Li, X., Xie, J., Yuan, X., and Xia, Y., Coating electrospun poly(ε-caprolactone) fibers with gelatin and calcium phosphate and their use as biomimetic scaffolds for bone tissue engineering, *Langmuir*, 2008, **24**, 14145-14150.

30. Bowers, D. T., Tanes, M. L., Das, A., Lin, Y., Keane, N. A., Neal, R. A., Ogle, M. E., Brayman, K. L., Fraser, C. L., and Botchwey, E. A., Spatiotemporal oxygen sensing using dual emissive boron dye-polylactide nanofibers, *ACS Nano*, 2014, **8**, 12080-12091.

31. Latour, R. A., Biomaterials: protein-surface interactions, *Encycl. Biomater. Biomed. Eng.*, 2005, 1-15.

32. Wright, A. K. and Thompson, M. R., Hydrodynamic structure of bovine serum albumin determined by transient electric birefringence, *Biophys. J.*, 1975, **15**, 137-141.

33. Kim, J. and Somorjai, G. A., Molecular packing of lysozyme, fibrinogen, and bovine serum albumin on hydrophilic and hydrophobic surfaces studied by infrared-visible sum frequency generation and fluorescence microscopy, *J. Am. Chem. Soc.*, 2003, **125**, 3150-3158.

34. Xie, J., Liu, W., MacEwan, M. R., Bridgman, P. C., and Xia, Y., Neurite outgrowth on electrospun nanofibers with uniaxial alignment: the effects of fiber density, surface coating, and supporting substrate, *ACS Nano*, 2014, **8**, 1878-1885.

35. Kapur, T. A. and Shoichet, M. S., Immobilized concentration gradients of nerve growth factor guide neurite outgrowth, *J. Biomed. Mater. Res. A*, 2004, **68**, 235-243.

36. Cao, X. and Shoichet, M. S., Defining the concentration gradient of nerve growth factor for guided neurite outgrowth, *Neuroscience*, 2001, **103**, 831-840.